Journal of Alloys and Compounds 696 (2017) 109–117

Contents lists available at ScienceDirect

Journal of Alloys and Compounds

journal homepage: http://www.elsevier.com/locate/jalcom

First-principles study of coherent interfaces of Laves-phase $MgZn_2$ and stability of thin $MgZn_2$ layers in Mg-Zn alloys

Xiao-Di Li, Hai-Tao Ma, Zhong-Hua Dai, Yi-Chen Qian, Li-Juan Hu, Yao-Ping Xie*

Key Laboratory for Microstructures and Institute of Materials Science, School of Materials Science and Engineering, Shanghai University, Shanghai 200072, China

ARTICLE INFO

Article history:
Received 2 September 2016
Received in revised form
11 November 2016
Accepted 16 November 2016
Available online 17 November 2016

Keywords:
Mg alloys
Precipitates
Laves-phase $MgZn_2$
Orientation relationships
First-principles calculations

ABSTRACT

The $\beta_1'$and β_2' are important precipitates in Mg-Zn alloys. Two types of precipitates both are composed of $MgZn_2$, but the orientation relationships of $MgZn_2$ with the α-Mg matrix in two precipitates are different. To understand the properties of $\beta_1'$and β_2', we use the first-principles method to perform a systematical investigation of coherent interfaces of β_1'/α-Mg and β_2'/α-Mg. Here, we present exhaustive analysis of the structure and stability for these interfaces, and find that the interfacial energy is highly dependent on the average coordination of interfacial structures. Furthermore, we find that the $MgZn_2$ slab in matrix with $[11\bar{2}\,0]_{MgZn2}//[0001]_\alpha$, $(0001)_{MgZn2}//(11\bar{2}\,0)_\alpha$ orientation relationship (OR1) is less stable than that with $[11\bar{2}\,0]_{MgZn2}//[10\bar{1}\,0]_\alpha$, $(0001)_{MgZn2}//(0001)_\alpha$ orientation relationship (OR2), which can explain that the β_2' plate shape precipitates that are frequently observed in Mg-Zn alloys comply with OR2 instead of OR1.

1. Introduction

Mg alloys, which offer a 30% weight reduction compared to aluminum alloys and a 75% weight reduction compared to steels, have received renewed attention due to the increasing demand to reduce carbon dioxide emissions in the transportation sector. One of drawbacks is that the strength of most commercial Mg alloys is relatively low. Precipitate hardening is an important strengthening method. It is known that ZK series alloys (Mg-Zn-Zr alloy) possess the greatest precipitation hardening among Mg-based alloys, but they still need to increase strength for industrial application [1–3]. Therefore, understanding its mechanism of precipitation is critical to improve the mechanic properties of existing alloys and design new alloys.

Pure Mg-Zn alloys whose grain size is large have almost no application in industry [4]. Eighty years ago, Sauerwald found that addition of Zr into Mg-Zn can change the precipitate in the grain boundary and refine the grain of the alloy, which efficiently improves the strengthening and ductile properties [5]. Now, the Mg-Zn-Zr alloy is one of the widest application wrought Mg-based alloys, and Mg–2.4Zn–0.16Zr (at. %, ZK60) is probably the material which has the highest specific strength. Though the ZK series alloys have a good combination of strength and ductility, the strength is still relatively low. For example, the yield strength of ZK60 is only 240 MPa [6,7], which is much lower than that of medium-strength Al alloys, 300 MPa [6].

Because of the lack of polymorphic transformation of Mg matrix in heat treatment, the solid-to-solid transition cannot be used to strengthen Mg alloys. The strengthening methods of Mg alloys include solid solution strengthening, grain boundary strengthening and precipitation strengthening. For wrought Mg alloys, the precipitates actually tightly influence both fine grain strengthening and precipitation strengthening. First, at the stage of hot extrusion and dynamic recrystallization process, the precipitate will inhibit the grain growth by pinning the grain boundaries and refine the grain size, which results in fine grain strengthening. Second, the precipitate can prevent the motion of dislocation and resist basal slip, which results in precipitation strengthening. Therefore, ZK series alloys have potential for heat-treatable precipitation hardening, but different ZK alloys hardening responses differ significantly [8]. For example, under the same heat treatment condition, the Mg–2.4Zn, Mg–2.4Zn–0.16Zr, Mg–2.4Zn–0.1Ca and Mg–2.4Zn–0.1Ag alloys have relative low hardness increment, 18, 15, 25 and 35 VH, while Mg–2.4Zn–0.1Ag–0.1Ca and Mg–2.4Zn–0.1Ag–0.1Ca–0.16Zr have relatively high hardness increment, 43 and 45 VH [3]. It indicates that the precipitation

* Corresponding author.
E-mail address: ypxie@shu.edu.cn (Y.-P. Xie).

http://dx.doi.org/10.1016/j.jallcom.2016.11.217
0925-8388/

strengthening can be changed by micro alloying, and it also provides a promising method to enhance the strength of Mg-based alloys. Therefore, to reveal the mechanism of precipitation in ZK alloys is not only a foundational issue, but also an emergent task in engineering fields.

The precipitation sequence in Mg-Zn based alloys during aging has been generally considered to occur as follows:

SSSS (super-saturated solid solution) → pre-β_1'/Guinier Preston (GP) zones → β_1' ($MgZn_2$, Mg_4Zn_7) → β_2' ($MgZn_2$) → β equilibrium phase (MgZn, Mg_2Zn_3).

β_1' and β_2' are the main strengthening phases [9]. β_1' occurs at peak-aged condition, while β_2' occurs at overage condition. It is now generally accepted that β_1' phase has $MgZn_2$ or Mg_4Zn_7 structures, while β_2' has the $MgZn_2$ structure. It is interesting that $MgZn_2$ can form both β_1' and β_2' phases. The main differences of two precipitated phases that are composed of $MgZn_2$ are shapes and orientation relationships (ORs). β_1' is rod shape, also named needle shape or lath shape, while β_2' is plate shape. The orientation relationships of two precipitated phases in alloys with different compositions are listed in Table 1.

In the theoretical side, because of the importance of strengthening effects of β_1' phase and the role of micro alloying on precipitation strengthening, the properties of $MgZn_2$ and Mg_4Zn_7 received extensive study. First, the basic properties such as crystal structure parameters, thermodynamic stability, elastic constants and electronic structures of $MgZn_2$ have been well studied [10]. Specially, many works compare the elastic properties of $MgZn_2$ with other similar intermediate phases, such as $MgNi_2$, $MgCu_2$, Mg_2Y, Mg_2Ca etc., to reveal the correlation of mechanical properties between the precipitation and matrix [11–15]. Second, to understand the effects of alloying elements on the microscopic structure, the effects of alloying elements and atomic vacancy on the stability of $MgZn_2$ and Mg_4Zn_7 also attract the attention [16]. Third, due to the importance of deformation properties of Mg alloys, the deformation mechanism of precipitates has been also investigated, and it was found that the deformation of $MgZn_2$ is performed by partial dislocations [17].

Most of studies above focus on the bulk properties of intermediate phase, but the precipitates embodied in the matrix inevitably have interfaces. In general, the phase structure, OR, density of precipitates, which are highly influenced by the precipitate interface, are predominant factors influencing the precipitation strengthening. For example, meta-stable precipitation phases, such as bcc Cu in Fe [18], β″-Mg_5Si_6 in Al [19], β_1'-$MgZn_2$ in Mg alloys [20,21], that form coherent interfaces with the matrix have the largest age-hardening responses. Finely dispersed precipitates with various habit planes usually have more effective precipitation hardening than precipitates with the same OR do. In addition, due to the importance of micro alloying, understanding the partition and segregation of alloy elements at the interface of precipitates is highly valuable [22,23], which also requests the knowledge of the interface structure. Therefore, a careful investigation of the interface between precipitates and matrix is very necessary.

To date, there are many TEM experiments revealing the interface structures between $MgZn_2$ and α-Mg matrix [9,25–31]. Table 1 lists the shapes and names of precipitate with two most common ORs, i.e., $[11\bar{2}\ 0]_{MgZn2}//[0001]_\alpha$, $(0001)_{MgZn2}//(11\bar{2}\ 0)_\alpha$ (OR1) and $[11\bar{2}\ 0]_{MgZn2}//[10\bar{1}\ 0]_\alpha$, $(0001)_{MgZn2}//(0001)_\alpha$ (OR2), in alloys with different compositions. Most authors named rod-like precipitates with OR1 as β_1', and named plate shaped with OR2 as β_2'. The coherent interface of β_1' precipitate parallel to $(0001)_{MgZn2}//(11\bar{2}\ 0)_\alpha$, while the coherent interface of β_2' precipitate parallel to $(0001)_{MgZn2}//(0001)_\alpha$. The first-principles method is a powerful tool to investigate precipitated phases and interfaces in alloys [33,34]. Since the properties of these two types of interfaces are critical to understand the β_1' and β_2' precipitates, in this paper, we use first-principles calculations preforming a systematical investigation of the structural properties of coherent interfaces of β_1' and β_2' in α-Mg alloys. We first describe the calculation details in section 2. Second, we present the interfacial energies of 16 coherent interfaces complying with OR1 and OR2, and describe the structural features of each interface by using coordination. We find that the interfacial energy is tightly influenced by the average coordination number of the interface structure. Third, we present the strain energies and formation energies for the slabs with different interfaces. Using results of formation energies, we explain the relative stability of β_1' and β_2'. Finally, we discuss the atomic structures and electronic structures of two favorable interfaces.

2. Methodology

In this paper, first-principles calculations based on density functional theory (DFT), within the generalized gradient approximation (GGA) [35] as incorporated in the Vienna Ab Initio Simulation Package (VASP) [36], are employed. The ion–electron interaction is described using the projector augmented wave (PAW) method [37,38]. A kinetic energy cut-off value of 280 eV was used for plane wave expansions. The Brillouin zone (BZ) integrations for

Table 1
The ORs, shapes and names of precipitates which are composed of $MgZn_2$ in alloys with different compositions.

Ref.	ORs	Name and shape of precipitates	Alloys
OR1			
Gallot [24] (1965)	$[11\bar{2}\ 0]_{MgZn2}//[0001]_\alpha$, $(0001)_{MgZn2}//(11\bar{2}\ 0)_\alpha$	β_1', rod-like	Mg-Zn
Singh [25] (2010)	$[11\bar{2}\ 0]_{MgZn2}//[0001]_\alpha$, $(0001)_{MgZn2}//(11\bar{2}\ 0)_\alpha$	β_2', rod-like	Mg-Zn-Y
Kim [26] (2010)	$[11\bar{2}\ 0]_{MgZn2}//[0001]_\alpha$, $(0001)_{MgZn2}//(11\bar{2}\ 0)_\alpha$	β_1', rod-like, lath	Mg-Zn-Y
Rosalie [27] (2010)	$[11\bar{2}\ 0]_{MgZn2}//[0001]_\alpha$, $(0001)_{MgZn2}//(11\bar{2}\ 0)_\alpha$	β_1', rod-like	Mg-Zn-Y
Zeng [28] (2006)	$[10\bar{1}\ 0]_{MgZn2}//[1\bar{1}\ 00]_\alpha$, $(0002)_{MgZn2}//(11\bar{2}\ 0)_\alpha$	β_1', rod-like	Mg-Zn-Al-Y
Park [29] (2007)	$[01\bar{1}\ 0]_{MgZn2}//[01\bar{1}\ 0]_\alpha$, $(2\bar{1}\bar{1}\ 0)_{MgZn2}//(0002)_\alpha$, $(0002)_{MgZn2}//(2\bar{1}\bar{1}\ 0)_\alpha$	β_1', rod-like	Mg–Zn–Mn–Al
Zou [30] (2008)	$[10\bar{1}\ 0]_{MgZn2}//[1\bar{1}\ 00]_\alpha$, $(0002)_{MgZn2}//(11\bar{2}\ 0)_\alpha$, $(1\bar{2}\ 10)_{MgZn2}//(0002)_\alpha$	β_1', rod-like	Mg-Zn-Al-Y
Shi [31] (2013)	$[01\bar{1}\ 0]_{MgZn2}//[01\bar{1}\ 0]_\alpha$, $(0001)_{MgZn2}//(\bar{2}\ 110)_\alpha$	β_1', needle-shaped	Mg-Zn-Sn
OR2			
Gallot [24] (1965)	$[11\bar{2}\ 0]_{MgZn2}//[10\bar{1}\ 0]_\alpha$, $(0001)_{MgZn2}//(0001)_\alpha$	β_2', plates	Mg-Zn
Komura [32] (1980)	$[11\bar{2}\ 0]_{MgZn2}//[10\bar{1}\ 0]_\alpha$, $(0001)_{MgZn2}//(0001)_\alpha$	β_2', plates	Mg-Zn
Wei [21] (1995)	$[11\bar{2}\ 0]_{MgZn2}//[10\bar{1}\ 0]_\alpha$, $(0001)_{MgZn2}//(0001)_\alpha$	β_2', plates	Mg-Zn-RE
Gao [9](2007)	$[11\bar{2}\ 0]_{MgZn2}//[10\bar{1}\ 0]_\alpha$, $(0001)_{MgZn2}//(0001)_\alpha$	β_2', plates	Mg-Zn

all calculations are performed by the special k-point sampling of the Gamma centered grid type. For Mg and Zn, the valence electrons considered are $3s^2$ and $3d^{10}4s^2$, respectively. The internal atoms in supercells are allowed to relax until the maximum forces on unconstrained atoms converged to less than 0.01 eV/Å.

We first calculate the lattice constants of α-Mg and $MgZn_2$. For the BZs of Mg and $MgZn_2$, we use the k-point meshes of $(8 \times 8 \times 4)$ and $(8 \times 8 \times 6)$, respectively. For pure α-Mg, our calculated lattice constants are 3.22 Å and 10.42 Å, which are well consistent with the experimental values, 3.21 Å and 5.21 Å. For $MgZn_2$, our calculated lattice constants are 5.20 Å and 8.43 Å, which are also well consistent with the experimental value 5.23 Å and 8.58 Å [9].

To study the properties of the Laves-phase $MgZn_2$, which complies with α-Mg matrix in different ORs, we construct different supercells to descript the interfacial structures. For interfaces with OR1 (Fig. 2(a)), we set $\vec{a}$ parallel to $[1\bar{1}00]_\alpha$ and $[1\bar{1}00]_{MgZn2}$, $\vec{b}$ parallel to $[0001]_\alpha$ and $[11\bar{2}0]_{MgZn2}$, and $\vec{c}$ parallel to $[11\bar{2}0]_\alpha$ and $[0001]_{MgZn2}$ for the supercells. For interfaces with OR2 (Fig. 2(b)), we set $\vec{a}$ parallel to $[21\bar{3}0]_\alpha$ and $[1000]_{MgZn2}$, $\vec{b}$ parallel to $[1\bar{1}00]_\alpha$ and $[01\bar{1}0]_{MgZn2}$, and $\vec{c}$ parallel to $[0001]_\alpha$ and $[0001]_{MgZn2}$ for the hexagonal supercells. The lengths of the lattice of supercells are illustrated in Fig. 2. We use a $(8 \times 4 \times 1)$ k-point mesh for the interfacial structures that comply with OR1 and a $(8 \times 8 \times 1)$ k-point mesh for the interfacial structures that comply with OR2 respectively.

Here, we use supercells with different Mg layers and the same $MgZn_2$ layers to test the influence of the thickness of Mg layers on the lattice constants parallel in the interfacial plane. Fig. 1 shows the dependence of calculated in-plane lattice constants with the number of Mg layers. We find that the in-plane lattice constants of the interface are strongly influenced by the number of Mg layers. With increasing Mg layers, the in-plane lattice constants approach the ideal lattice of bulk Mg (5.58 Å). We can infer that in-plane lattice constants of the interface between $MgZn_2$ and α-Mg matrix must be the same with that of bulk α-Mg. There are two strategies to simulate the interface: one is using a very large thickness of Mg layers to emulate the real α-Mg matrix, and it at least needs Mg layers with thickness larger than 50 layers, which needs a very huge computational expenditure. To avoid huge computational expenditure, another strategy that we adopt here is using a relatively thin matrix (4 layers of Mg) and directly set the in-plane lattice constants as the same with our calculated value of Mg bulk lattice; we implement a series of static total energy calculation to scan the energy profile along the $\vec{c}$ direction of supercells and determine the favorable interfacial structure. This method has been widely used to simulate the coherent interface of precipitates in alloys. For example, thin slabs are used to emulate the real alloy matrix in the models, which simulate the coherent interfaces of Al_2Cu in the Al-Cu alloys [39,40], γ′-Ni_3Al in γ-Ni [41], Al_2MgC_2 in Mg alloys [42] and Al_4C_3 in Mg alloys [43]. The interface properties, such as the interfacial energy and segregation behavior etc., are mainly influenced by chemical bonding at the interface, which is only determined by the nearest neighbor of the interfacial atoms, while the atoms far from the interface have no influence on the interfacial properties (We can also find that the coordination number, which reflects the number of nearest neighbor atoms, has the same variation trend as interfacial energy in section 3.3.). Therefore, a thin slab of matrix can be used to construct the structure of the coherent interface of precipitates in alloys.

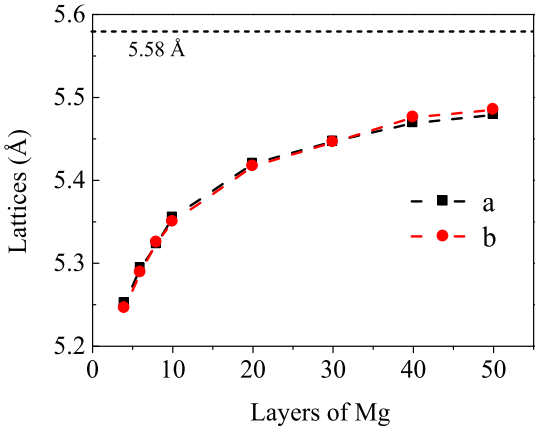

Fig. 1. The dependence of calculated in-plane lattice parameters of Mg(0001) plane on the thickness of Mg layers within supercells simulating interfaces.

The formation energy (E_f) reflects the stability of a given structure, which is given by:

$$E_f = E_{Int} - N1_{Mg}E_{Mg} - N_{MgZn2}E_{MgZn2} - N2_{Mg}E_{Mg} - N2_{Zn}E_{Zn} \quad (1)$$

where E_{Int} represents the total energy of the supercell, E_{Mg} and E_{Zn} represent the energy per atom of Mg and Zn in their equilibrium states respectively. E_{MgZn2} represents the energy of the stoichiometric part $MgZn_2$ in equilibrium state. $N1_{Mg}$ and N_{MgZn2} represent the number of Mg atoms in α-Mg layers and the number of atoms of stoichiometric part $MgZn_2$ in the supercell, respectively. $N2_{Mg}$ and $N2_{Zn}$ respectively represent number of Mg and Zn atoms in $MgZn_2$ except for the stoichiometric part. It is worth to mention that, in all simulations of the interfaces, we use symmetrical structures in supercells that contain two equivalence interfaces to compute the interface formation energy. The slabs in these supercells simulating interfaces would have different thickness of $MgZn_2$ slabs (see Table 2).

The formation energy as defined in Eqn. (1) contains contributions from both the interfacial energy and the elastic strain energy. Therefore, the formation energy of Eqn. (1) can be also expressed as following equation:

Table 2
The average coordination of Mg and Zn of the interface: N_C^{all} is the average coordination of all atoms in the cell, N_C^{Mg} is the average coordination of all Mg atoms in the cell, N_C^{Zn} is the average coordination of all Zn atoms in the cell. C represents the Zn concentration in the $MgZn_2$ part, and L represents the thickness of $MgZn_2$ slab in the interfacial structure.

	N_C^{all}	N_C^{Mg}	N_C^{Zn}	C (at. %)	L (Å)
Mg	12.00	12.00	0	0	–
$MgZn_2$	13.33	16.00	12.00	66.67	–
OR1 interface					
I_1	13.13	14.34	12.20	69.23	25.76
I_2	12.83	13.38	12.31	63.64	22.19
I_3	13.00	13.97	12.17	67.74	21.30
I_4	12.87	13.50	12.26	65.52	19.18
I_5	13.00	14.16	12.03	70.37	18.24
I_6	13.21	13.72	12.58	61.90	13.85
I_7	12.74	13.57	11.85	68.42	13.68
I_8	12.24	12.54	11.86	64.70	11.76
OR2 interface					
I_1	13.10	14.33	12.00	69.23	27.39
I_2	12.89	13.67	12.00	63.64	23.48
I_3	12.37	13.27	11.43	67.74	22.85
I_4	13.07	14.00	12.00	65.52	20.53
I_5	12.62	13.50	11.68	70.37	18.97
I_6	12.73	13.20	12.00	61.90	15.26
I_7	12.00	12.67	11.08	68.42	14.63
I_8	12.97	13.56	12.00	64.71	12.21

$$E_f = \sigma + \zeta \tag{2}$$

where σ represents the interfacial energy, and ζ is the elastic strain energy.

The elastic strain energy of the interface is due to the lattice mismatch of $MgZn_2$ with α-Mg matrix. Since we use the thin slab of $MgZn_2$ in Mg layers to simulate precipitate in alloys, in which the thickness of $MgZn_2$ is much thinner than that of matrix, the influence of strain on the matrix is negligible. From Fig. 1, we also find that, for a thin slab of $MgZn_2$ model, the lattice constants of thick Mg layers almost are the same with those of its equilibrium state. Therefore, strain of the interface can be computed by only considering the strain of the $MgZn_2$ part. The strain energy ζ of the supercell can be calculated by following equation:

$$\zeta = E_{st} - E_{op} \tag{3}$$

where E_{st} represents the total energy of $MgZn_2$ slab with same distortion in the supercell simulating interface, and E_{op} is the total energy of $MgZn_2$ slab with same lattice as equilibrium state.

3. Results and discussion

3.1. Interface structures

Fig. 2(a) shows the $(11\bar{2}0)$Mg plane and (0001)$MgZn_2$ plane (OR1 interface) and Fig. 2(b) shows the (0001)Mg plane and (0001) $MgZn_2$ plane (OR2 interface). Clearly, the (0001)$MgZn_2$ can easily form coherent interface with both $(11\bar{2}0)$Mg and (0001)Mg planes. The mismatch of OR1 and OR2 interfaces are 19.29% and 13.16%, respectively. Due to the complicate structure of $MgZn_2$, the truncated surface of $MgZn_2$ has 8 different confirmations (see Figs. 3 and 4). Therefore, both OR1 and OR2 coherent interfaces have 8 different structures, which are denoted as I_1-I_8 in Figs. 3 and 4 respectively.

3.2. Stability of interfaces

Using Eqns. (1)–(3), we obtain the interfacial energies for OR1 and OR2 interfaces, which are shown in Fig. 5. The interfacial energies of OR1 interfaces are among −4.9–34.2 meV/Å^2, and the interfacial energies of OR2 interfaces are among −2.7–49.7 meV/Å^2. The OR1-I_4, OR1-I_6 and OR2-I_1 interfaces are three most stable energy interfaces, whose interfacial energies are −2.4, −4.9 and −2.7 meV/Å^2, respectively. The OR2-I_3 and OR2-I_7 are two least stable interfaces, whose interface energies are 49.8 and 46.8 meV/Å^2, respectively. Though the mismatch of OR2 is much little than that of OR1 interfaces, the interfacial energy of OR2 type is not always lower than that of OR1 type. The most stable OR1-I_6 interface is even lower than that of OR2-I_1. Therefore, the interface stability between $MgZn_2$ and α-Mg must relate to the bonding formation at the interface, due to the diversity of the structures truncated surface $MgZn_2$.

3.3. Interface coordination

To reveal the bonding numbers in the interfacial structures, we compute the average coordination for all atoms in these interfaces, N_C^{all}. Also, we compute the average coordination for all Mg and Zn atoms in these interfaces, N_C^{Mg} and N_C^{Zn}, respectively. The coordination number N_C^A is defined as follow:

$$N_C^A = \frac{1}{N_0^A}\sum_{i=1}^{N_0^A}\sum_{j=1(i\neq j)}^{N}\lim_{k\to\infty}\frac{1}{1+\exp\left[-2k(d_{i,j}-d_0)\right]} \tag{4}$$

N_0^A is the number of A (A = Mg, Zn, Mg + Zn) atoms in the supercell, N is the total number of atoms in the supercell, i and j are the atom labels, $d_{i,j}$ is the distance between the i atom and j atom, d_0 is a constant equal to 4.0 (Å). The N_C^A actually reflects the average number of nearest neighbor atoms around A atoms in the structure, therefore it can reflect the bonding number around A atom in the structure. We list the average coordination numbers, Zn concentration in $MgZn_2$ part, and the thickness of $MgZn_2$ slab in the interfaces in Table 2, and these data are useful to describe the feature of interfaces.

The average coordination of all atoms in Mg and $MgZn_2$ are 12.00 and 13.33, respectively. Naturally, the average coordination of all atoms (N_C^{all}) in the structures for OR1 and OR2 interfaces are between 12.00 and 13.33. It is found that the concentration (C) of Zn in $MgZn_2$ part which used to construct the interface is different from that of stoichiometric $MgZn_2$. We notice that the thicknesses of slab of $MgZn_2$ part (L) for constructing different interfaces also have a relatively large difference (The thickness of Mg layers in all interfaces is the same, so the thickness of $MgZn_2$ can reflect the concentration of $MgZn_2$ in supercells). However, the average coordination for the interface is not a monotonic function of the concentration of Zn in $MgZn_2$ or thickness of the $MgZn_2$ slab. Therefore, we can infer that the average coordination of all atoms in these structures should be influenced by the complicated structure of truncated surface, which introduces many atoms with different

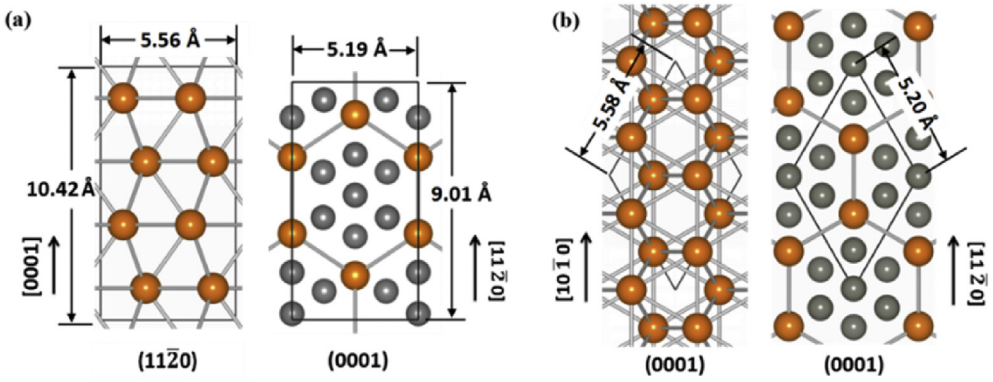

Fig. 2. The parallel planes from Mg and $MgZn_2$ for interfaces: (a) OR1 interface, (b) OR2 interface. The orange balls represent Mg atoms, the dark grey balls represent Zn atoms, the light grey sticks represent the Mg-Mg bonds, and the solid black lines are the boundaries of supercells. For clarity, we do not plot the bonds of Mg-Zn and Zn-Zn. (For interpretation of the references to colour in this figure legend, the reader is referred to the web version of this article.)

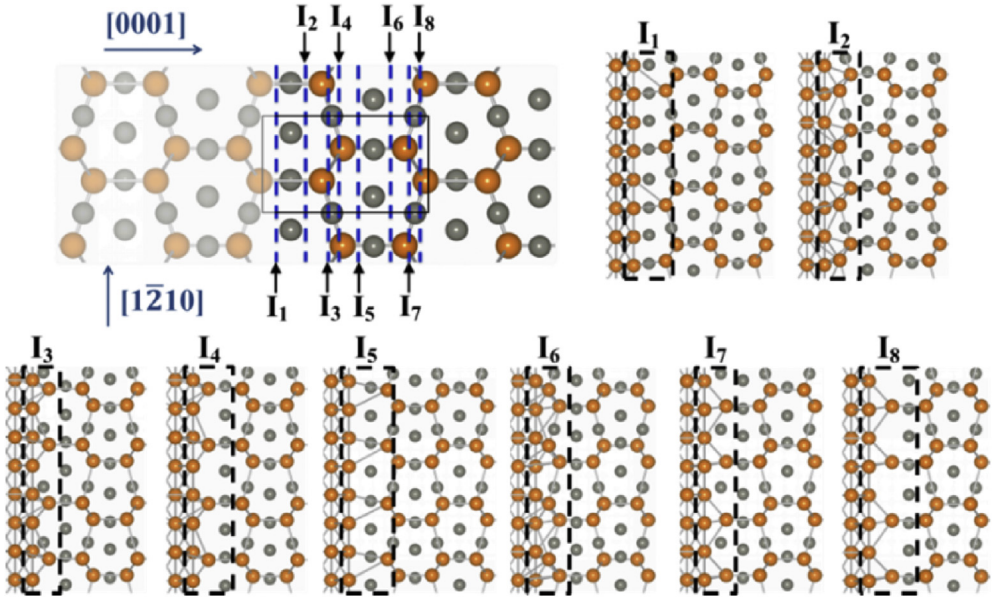

Fig. 3. The atomic structure of coherent interface $(0001)_{MgZn2}//(11\bar{2}\,0)_{\alpha}$ complying with OR1. The blue dashed lines marked by (I_1-I_8) are the truncated planes of $MgZn_2$ which appear in the slab used to construct interfaces in right and bottom panels. (For interpretation of the references to colour in this figure legend, the reader is referred to the web version of this article.)

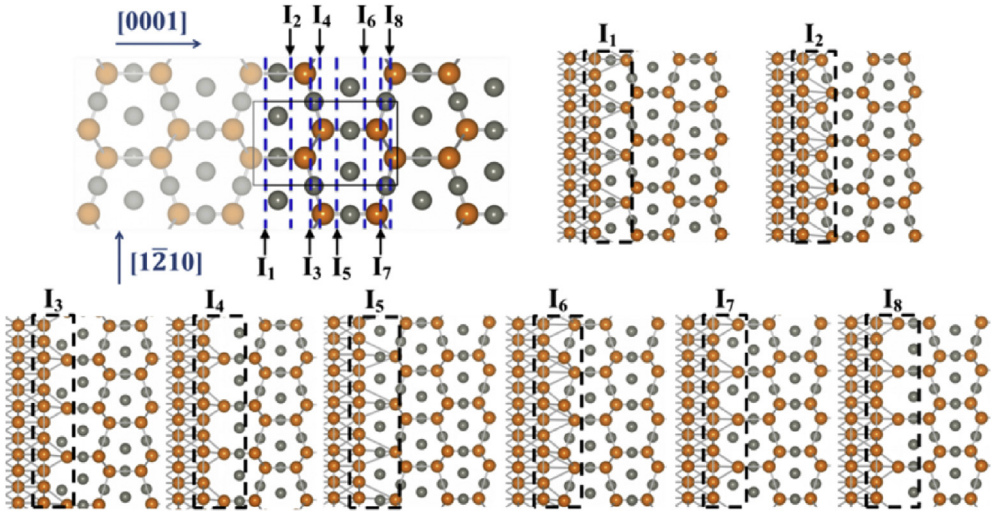

Fig. 4. The atomic structure of coherent interface $(0001)_{MgZn2}//(0001)_{\alpha}$ complying with OR2. The blue dashed lines marked by (I_1-I_8) are the truncated planes of $MgZn_2$ which appear in the slab used to construct interfaces in right and bottom panels. (For interpretation of the references to colour in this figure legend, the reader is referred to the web version of this article.)

coordination numbers.

Because both components, Mg and $MgZn_2$, of the interface include Mg atoms, the average coordination of Mg atoms (N_C^{Mg}) of the interface depends on both the thickness of $MgZn_2$ and the structure of the truncated surface. In contrast, Zn atoms only exist in $MgZn_2$, therefore the average coordination of Zn atoms (N_C^{Zn}) just depends on the structure of the truncated surface. We stress the role of N_C^{Zn} to reveal the interfacial structure feature is more important than that of N_C^{Mg}. Interestingly, we find that the number of average coordination of Zn atoms of most OR1 interfaces (except I_7 and I_8) is even larger than that of $MgZn_2$. For OR2 interface, all the average coordination number of Zn atoms is not larger than that of $MgZn_2$. The average coordination of Zn atoms can actually reflect the atom density at the interface. For example, the atom density at OR1-I_6 interface, whose N_C^{Zn} is 12.58, is much greater than that at OR1-I_7 and OR1-I_8, whose N_C^{Zn} respectively are 11.85 and 11.86 (See Fig. 3).

3.4. Coordination vs. interfacial energy

The average coordination can reflect the average number of bonding in structures. The larger the average coordination number of the structure is, the more bonds the structure has, and the lower total energy the structure is. Here N_C^{all} can mainly reflect the bonding around both Mg and Zn, which is influenced by the interface, and N_C^{Zn} exactly reflect the bonding around Zn at the interface. For example, the two most stable OR1-I_6 and OR2-I_1 interfaces have the two largest values of N_C^{all}, 13.21 and 13.10, while

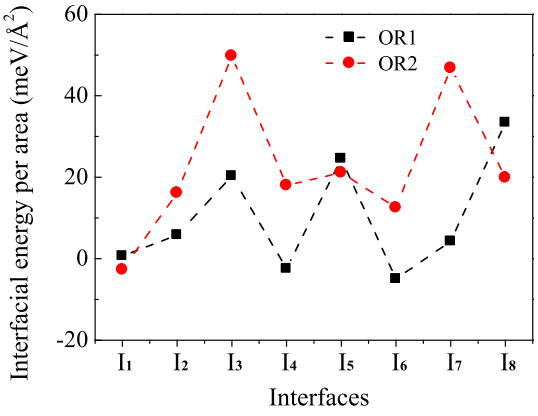

Fig. 5. Interfacial energies of interfaces that comply with OR1 and OR2.

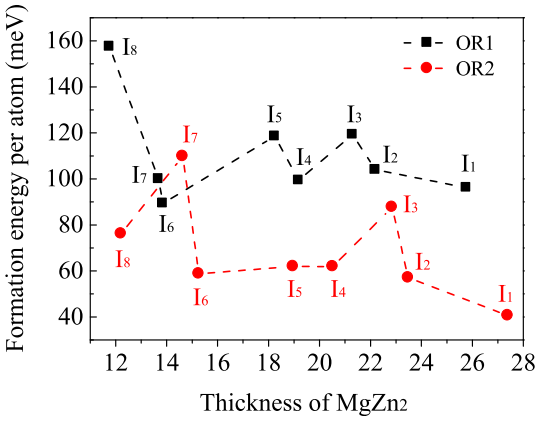

Fig. 7. Formation energies of $MgZn_2$ slabs with interfaces that comply with OR1 and OR2.

the two least stable OR1-I_8 and OR2-I_7 interfaces have the two smallest values of N_C^{all}, 12.24 and 12.00. Also, the most two stable OR1-I_6 and OR2-I_1 interfaces have the largest two values of N_C^{Zn}, 12.58 and 12.00, while the least stable OR2-I_3 and OR2-I_7 interfaces have the smallest two values of N_C^{Zn}, 11.43 and 11.08. However, though N_C^{Mg} can reflect the bonding number around Mg atoms, it is greatly influenced by the proportions of Mg and $MgZn_2$, causing N_C^{Mg} cannot directly reflect change of bonding number influenced by the interface. Therefore, N_C^{Mg} cannot reflect the change of interfacial energy. For example, the coordination value N_C^{Mg} of the most stable OR1-I_6 interface is 13.72, which is smaller than that of OR1-I_1 that is less stable, 14.34.

3.5. Strain energy and formation energy

Using Eqn. (3) we can obtain the strain energies of the slabs used to simulate interfaces. From Fig. 6, we find that the strain energy has a rough linear relation with atomic number in the slab of $MgZn_2$. The average strain energy per atom of OR1 and OR2 are 0.10 and 0.046 eV/atom, respectively. The reason why the strain energy of OR1 interface is larger than that of OR2 interface is the mismatch of OR1 interface is larger than that of OR2 interface.

The formation energy, which is the sum of the interfacial energy and strain energy, determines the stability of the precipitates. Fig. 7 presents the average formation energy per atom of $MgZn_2$ slabs with OR1 and OR2 interfaces. The formation energies of slabs with OR1 interfaces are among 89.41–157.49 eV/atom, while the formation energies of slabs with OR2 interfaces are among 40.61–109.83 eV/atom. The most stable slab with the OR1 interface is the slab with interface OR1-I_6, while the most stable slab with OR2 is the slab with OR2-I_1. It is found that most of the $MgZn_2$ slabs with OR2 interfaces are much more stable than those slabs with OR1 interfaces when the slab thickness is from 11 to 28 Å. However, the formation energies of the slab with OR2-I_3 and OR2-I_7 are 87.73 meV/atom and 109.83 meV/atom, respectively, which are comparable to and even exceed that of the slab with OR1-I_6, 89.41 meV/atom, indicating the slab with OR2-I_3 and OR2-I_7 are unfavorable compared to other slabs with OR2 having thickness among 12–28 Å. This energetics can well explain that the β_2' plate shape precipitates that are frequently observed have OR2 relationship instead of OR1 [9,21,22,30]. It also indicates that β_2' is more stable than β_1', which is consistent with experiments.

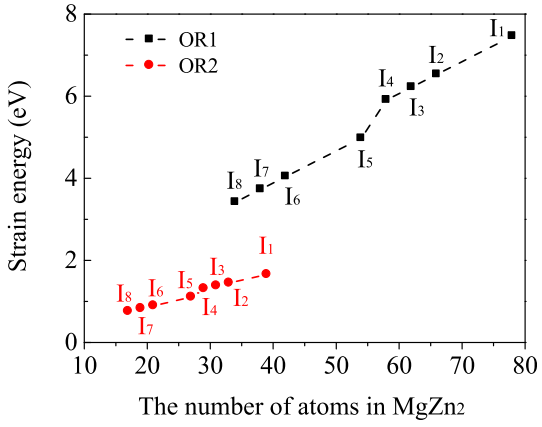

Fig. 6. Strain energies of interfaces that comply with OR1 and OR2.

3.6. The structures of OR1-I_6 and OR2-I_1 interfaces

Fig. 8 presents the atomic structures of the most stable interfaces for OR1 and OR2, namely OR1-I_6 and OR2-I_1, respectively. Fig. 8(a and b) show the unrelaxed atomic position and optimized atomic position of cross-section along the basal plane of $MgZn_2$ for OR1-I_6 interface, and we find there is obvious reconstruction in this interface. In contrast, from Fig. 8(d and e), which show the unrelaxed atomic position and optimized atomic position in the cross-section along the basal plane of $MgZn_2$ for the OR2-I_1 interface, we find there is almost no reconstruction. The atomic configurations in cross-sections along prism planes of $MgZn_2$ of unrelaxed and relaxed planes are also presented in Fig. 8(c, f), which also indicate that OR1-I_6 has obvious reconstruction but OR2-I_1 almost has no reconstruction.

Table 3 lists the coordination numbers of interfacial atoms, which are marked in Fig. 8, of ORI-I_6 and OR2-I_1 interfaces. We describe the features of OR1-I_6 and OR2-I_1 respectively as following:

3.6.1. OR1-I_6

Compared to atoms in the corresponding single phase (α-Mg or $MgZn_2$), the coordination number of interfacial Mg atoms at α-Mg side all becomes larger, while that of interfacial Mg atoms at $MgZn_2$ side all becomes smaller. The total number of coordination of all these interfacial Mg atoms decreases by 1. Most of the coordination of interfacial Zn atoms becomes larger compared to that of the $MgZn_2$ phase. The total number of coordination of all these interfacial Zn atoms increases by 5. The total number of coordination of all atoms of this interface will increase by 4. Now, it is clear that the

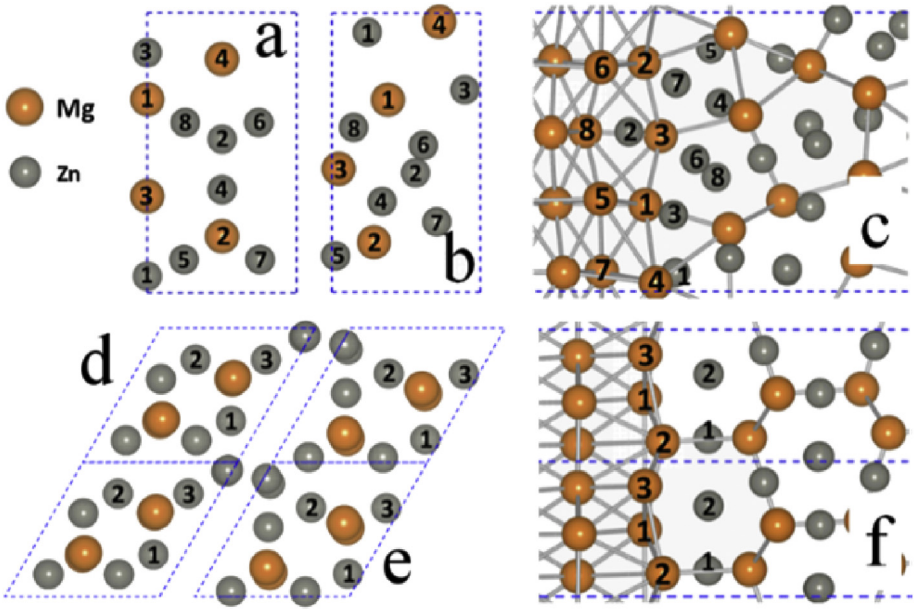

Fig. 8. The structures of interfaces OR1-I_6 (a, b and c) and OR2-I_1 (d, e, and f): (a, d) show the atomic configuration of cross-section parallel to basal plane of $MgZn_2$ for unrelaxed interfacial structure, (b, e) show the atomic configuration of cross-section parallel to basal plane of $MgZn_2$ for relaxed interfacial structure, and (c, f) show the atomic configuration of cross-section parallel to prism plane of $MgZn_2$ for relaxed interfacial structure.

Table 3
The coordination numbers (N_C^{all}) of interfacial atoms that marked in Fig. 8.

OR1-I_6							
Mg1	Mg2	Mg3	Mg4	Mg5	Mg6	Mg7	Mg8
14	15	15	16	13	13	13	12
Zn1	Zn2	Zn3	Zn4	Zn5	Zn6	Zn7	Zn8
11	13	13	15	13	12	12	13
OR2-I_1						$MgZn_2$	
Mg1	Mg2	Mg3	Zn1	Zn2	Zn3	Mg	Zn
12	16	12	12	12	12	16	12

increase of total coordination number of this interface is because of the contribution of Zn atoms. Therefore, due to the atoms in this interface providing more chemical bonds compared to the $MgZn_2$ phase, interfacial Zn atoms involve in the enhancement of interface cohesion, which also leads to a very low interfacial energy.

3.6.2. OR2-I_1

The coordination numbers of all interfacial atoms, except Mg2, are the same with the corresponding single phase. Since only the coordination number of Mg2 increase by 4 compared to single phase α-Mg, the total coordination number of this interface also increases by 4 compared to the corresponding single phase. Therefore, the increase of coordination of this interface is due to the contribution of the Mg2 atom, and the Mg2 atom is a strong joint point for OR2-I_1.

Fig. 9(a and b) show the local densities of states (LDOS) of the interfacial atoms. Here, we sum up the LDOS of all Mg atoms and Zn atoms at the interfaces, which are marked in Fig. 8. It is shown that the LDOS of Mg is delocalized because the valence electronic states of Mg atoms are all s and p states, while the LDOS of Zn is more localized because the valence electronic states of Zn atoms are mainly d states. The localized states usually are the main contributors to chemical bonds. Here, it is found that the peak of the d states of Zn atoms at the interface is closer to the Fermi level compared to that of Zn atoms in the equilibrium state of $MgZn_2$. In addition, the states of Mg atoms are also closer to the Fermi level compared to that of Mg atoms in the equilibrium state of $MgZn_2$. The shallower electronic bands of interfaces, especially for d-band of Zn atoms, compared to that of the equilibrium state, indicate the higher bonding energies and weaker bonding strength, which is induced by the stretch of the bond length. For example, the Zn-Zn bond lengths around Zn6 in OR1-I_6 are 2.65, 2.69, 2.72, 2.76, 2.80, 2.98 and 3.12 Å, which are obviously larger than the Zn-Zn bond lengths (2.60, 2.61, 2.68, 2.68, 2.83 and 2.83 Å) in the equilibrium state of $MgZn_2$.

As mentioned in the previous section, the in-plane stretch of OR1-I_6, 19.29%, is larger than that of OR2-I_1, 13.16%. To verify the reason of the formation of relatively high energy electronic bands of atoms at the interface, we present LDOS of the $MgZn_2$ phase with the same extent of stretch along the basal plane as the interface, which is shown in Fig. 9(c and d). We find that the peak of the d states of Zn atoms and band bottom of Mg atoms in the stretched phase are also closer to the Fermi level than the peak of the d states of Zn atoms and band bottom of Mg atoms in the equilibrium state of $MgZn_2$, respectively.

For a detail survey, we estimate the band centers of d-bands of Zn, which are marked in Fig. 9(b, d). We find that the d-band centers of bands of Zn for two interfaces are both higher than that of Zn in equilibrium phase. The center of d-band of Zn in interface OR1-I_6 that has relatively large in-plane stretch is higher than that of Zn in interface OR2-I_1 by 0.12 eV. Similarly, the d-band centers of bands of Zn for stretched phases are both higher than that of Zn in equilibrium phases. The center of d-band of the stretched phase that has relatively large stretch is higher than that of Zn in the stretched phase that has relatively small stretch by 0.08 eV, which approach the value of energy difference between d-band centers of Zn atoms in OR1-I_6 and OR2-I_1. Therefore, we can confirm the change of bands of Zn atoms of the interface is induced by the structure distortion and bonding stretch.

It is also found that the band bottom of Mg atoms at OR2-I_1 is higher than that of Mg atoms in equilibrium state by 0.77 eV, and band bottom of Mg atoms at OR1-I_6 is higher than that of Mg atoms in OR2-I_1 by only 0.21 eV. Similarly, the band bottom of Mg atoms in

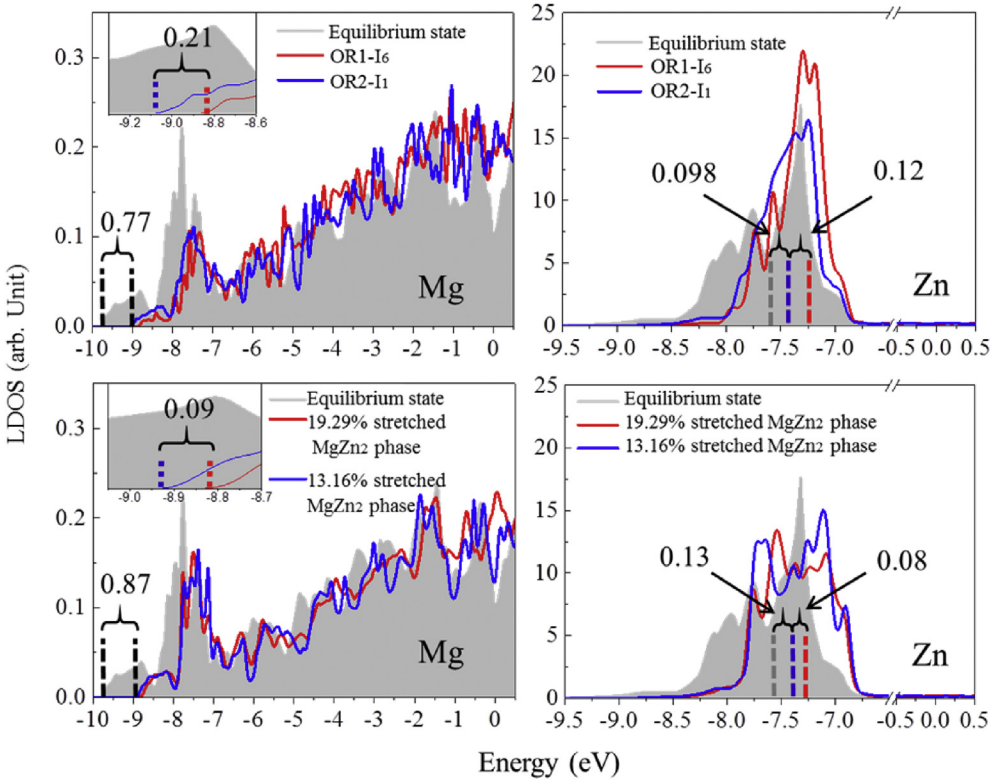

Fig. 9. The local density of states (LDOS) of Mg and Zn atoms within interface and $MgZn_2$ with stretch in basal plane: (a, b) illustrate the LDOS of Mg and Zn atoms for the interface respectively, and (c, d) illustrate the LDOS of Mg and Zn atoms for $MgZn_2$ with stretch in basal plane respectively. The number (in eV) in each panel is the difference of energies between electronic bands.

the 13.16% stretched phase is higher than that of Mg atoms in the equilibrium state by 0.87 eV, and band bottom of Mg atoms in the 19.29% stretched phase is higher than that of Mg atoms in the 13.16% stretched phase by only 0.09 eV. The similar changes of electronic states of Mg atoms in interfaces and stretched phases also reflect that the change of LDOS energy is mainly contributed by the structure distortion and bonding stretch.

From the LDOS of interfaces, we can infer that the bonding energy within the interface is higher than that within equilibrium $MgZn_2$, which has an effect on increasing the interfacial energy. However, from the coordination of OR1-I_6 and OR2-I_1, the bonding number for interfacial atoms increases, which has an effect on decreasing the interfacial energy. The effect of bonding number is much larger than the change of bonding energy induced by the distortion, and therefore the interfacial energies of these two interfaces are negative.

4. Summary

Using first-principles calculations to perform a systematic study on the coherent interfaces belong to β_1' and β_2' precipitates, $(0001)_{MgZn2}//(11\bar{2}\,0)_\alpha$ and $(0001)_{MgZn2}//(0001)_\alpha$. The conclusions can be summarized as following:

1. The most stable interface of β_1'/α-Mg is OR1-I_6, while the most stable interface of β_2'/α-Mg is OR2-I_1. The interfacial energy of OR1-I_6 is lower than that of OR2-I_1, because the OR1-I_6 structure has more average coordination than that of OR2-I_1.
2. The interfacial energy is highly influenced by the coordination of the interface structure, but is less influenced by the energy of bonding between atoms at the interface compared to coordination.
3. The strain energies of the slabs with interfaces that comply with given OR have a linear relationship with the atom numbers of $MgZn_2$ in slabs, and the values of the strain energy per atom in the slabs with given OR are almost constant.
4. Most of the $MgZn_2$ slabs with OR2 interfaces are more stable than that with OR1 interfaces, which explains that the β_2' plate shape precipitates that are frequently observed have OR2 relationship instead of OR1. It also indicates that β_2' is more stable than β_1', which is consistent with experiments.
5. Electronic analysis shows that the energy of bonding between atoms in the OR1-I_6 interface is higher than that in OR2-I_1, and the reason is that OR1-I_6 has larger bond stretch than OR2-I_1 does.

Acknowledgements

This work is supported by Science and Technology Commission of Shanghai Municipality (15ZR1416000) and National Science Foundation of China (51301102). The computations were performed at Ziqiang Supercomputer Center of Shanghai University.

References

[1] K. Hono, C.L. Mendis, T.T. Sasaki, K. Oh-ishi, Towards the development of heat-treatable high-strength wrought Mg alloys, Scr. Mater. 63 (7) (2010) 710–715.
[2] J.F. Nie, Precipitation and hardening in magnesium alloys, Metall. Mater. Trans. A 43 (11) (2012) 3891–3939.
[3] H.Z. Ye, X.Y. Liu, Review of recent studies in magnesium matrix composites, J. Mater. Sci. 39 (20) (2004) 6153–6171.
[4] J. Peng, B.J. Lv, F.S. Pan, D.F. Zhang, Advances in high plasticity Mg-Zn-based rare-earth magnesium alloys, Mater. Heat Treat. 39 (2010) 15–19.
[5] W.P. Sanunders, E.P. Strieter, Alloying zirconium to magnesium, Trans. Am.

foundrymen's Soc. 60 (1952) 581–594.
[6] I.J. Polmear, Light Metals, fourth ed., Butterworth Heinemann, Oxford, 2006.
[7] M.M. Avedesian, H. Baker, ASM Specialty Handbook: Magnesium and Magnesium Alloys, ASM International, Materials Park, OH, 1999.
[8] C.L. Mendis, K. Oh-ishi, Y. Kawamura, T. Honma, S. Kamado, K. Hono, Precipitation-hardenable Mg–2.4Zn–0.1Ag–0.1Ca–0.16Zr (at.%) wrought magnesium alloy, Acta Mater. 57 (3) (2009) 749–760.
[9] X. Gao, J.F. Nie, Characterization of strengthening precipitate phases in a Mg–Zn alloy, Scr. Mater. 56 (8) (2007) 645–648.
[10] M.M. Wu, L. Wen, B.Y. Tang, L.M. Peng, W.J. Ding, First-principles study of elastic and electronic properties of $MgZn_2$ and $ScZn_2$ phases in Mg–Sc–Zn alloy, J. Alloys Compd. 506 (1) (2010) 412–417.
[11] Q. Chen, Z. Huang, Z. Zhao, D. Shu, First principles study on elastic properties, thermodynamics and electronic structural of AB_2 type phases in magnesium alloy, Solid State Commun. 162 (2013) 1–7.
[12] P.L. Mao, B. Yu, Z. Liu, F. Wang, Y. Ju, Mechanical properties and electronic structures of $MgCu_2$, Mg_2Ca and $MgZn_2$ Laves phases by first principles calculations, Trans. Nonferrous Metals Soc. China 24 (9) (2014) 2920–2929.
[13] Y. Liu, H. Ren, W.C. Hu, D.J. Li, X.Q. Zeng, K.G. Wang, J. Lu, First-principles calculations of strengthening compounds in magnesium alloy: a general review, J. Mater. Sci. Technol. (2016), http://dx.doi.org/10.1016/j.jmst.2016.04.003.
[14] Y. Liu, W.-C. Hu, D.-J. Li, X.-Q. Zeng, C.-S. Xu, Theoretical predictions of the structural and thermodynamic properties of $MgZn_2$ Laves phase under high pressure, Appl. Phys. A 115 (1) (2014) 323–331.
[15] Y. Liu, W.C. Hu, D.J. Li, X.Q. Zeng, C.S. Xu, X.-J. Yang, First-principles investigation of structural and electronic properties of $MgCu_2$ Laves phase under pressure, Intermetallics 31 (2012) 257–263.
[16] Y.P. Xie, Z.Y. Wang, Z.F. Hou, The phase stability and elastic properties of $MgZn_2$ and Mg_4Zn_7 in Mg–Zn alloys, Scr. Mater. 68 (7) (2013) 495–498.
[17] L. Ma, T.W. Fan, B.Y. Tang, L.M. Peng, W.J. Ding, Ab initio study of I_2 and T_2 stacking faults in C14 Laves phase $MgZn_2$, Eur. Phys. J. B 86 (4) (2013) 1–5.
[18] S.K. Lahiri, D. Chandra, L.H. Schwartz, M.E. Fine, Modulus and Mossbauer studies of precipitation in Fe-1.67at. pct Cu, Trans. Metall. Soc. Aime 245 (9) (1969), 1865-&.
[19] Y. Wang, Z.K. Liu, L.Q. Chen, C. Wolverton, First-principles calculations of β″-Mg_5Si_6/α-Al interfaces, Acta Mater. 55 (17) (2007) 5934–5947.
[20] X. Zeng, Y. Zhang, C. Lu, W. Ding, Y. Wang, Y. Zhu, Precipitation behavior and mechanical properties of a Mg–Zn–Y–Zr alloy processed by thermo-mechanical treatment, J. Alloys Compd. 395 (1) (2005) 213–219.
[21] L.Y. Wei, G.L. Dunlop, H. Westengen, The intergranular microstructure of cast Mg-Zn and Mg-Zn-rare earth alloys, Metall. Mater. Trans. A 26 (8) (1995) 1947–1955.
[22] C.K. Ande, M.H.F. Sluiter, First-principles prediction of partitioning of alloying elements between cementite and ferrite, Acta Mater. 58 (19) (2010) 6276–6281.
[23] J. Wang, R. Janisch, G.K.H. Madsen, R. Drautz, First-principles study of carbon segregation in bcc iron symmetrical tilt grain boundaries, Acta Mater. 115 (2016) 259–268.
[24] J. Gallot, R. Graf, New observations with X-ray and electron microscope on the transitional phase occurring in the magnesium-zinc alloy with 6% zinc, Acc. Render. Acda. Sci. B 261 (3) (1965), 728-&.
[25] A. Singh, J.M. Rosalie, H. Somekawa, T. Mukai, The structure of precipitates in Mg–Zn–Y alloys, Philos. Mag. Lett. 90 (9) (2010) 641–651.
[26] W.J. Kim, S.I. Hong, K.H. Lee, Structural characterization of Laves-phase $MgZn_2$ precipitated in Mg-Zn-Y alloy, Metals Mater. Int. 16 (2) (2010) 171–174.
[27] J.M. Rosalie, H. Somekawa, A. Singh, T. Mukai, Structural relationships among $MgZn_2$ and Mg_4Zn_7 phases and transition structures in Mg-Zn-Y alloys, Philos. Mag. 90 (24) (2010) 3355–3374.
[28] X. Zeng, H. Zou, C. Zhai, W. Ding, Research on dynamic precipitation behavior of pre-solution treated Mg-5wt.% Zn-2wt.% Al (-2wt.% Y) alloy during creep, Mater. Sci. Eng. A 424 (1) (2006) 40–46.
[29] S.S. Park, Y.S. Oh, D.H. Kang, N.J. Kim, Microstructural evolution in twin-roll strip cast Mg–Zn–Mn–Al alloy, Mater. Sci. Eng. A 449 (2007) 352–355.
[30] H.H. Zou, Effects of microstructure on creep behavior of Mg-5% Zn-2% Al (-2% Y) alloy, Trans. Nonferrous Metals Soc. China 18 (3) (2008) 580–587.
[31] Z.Z. Shi, W.Z. Zhang, Enhanced age-hardening response and microstructure study of an Ag-modified Mg–Sn–Zn based alloy, Philos. Mag. Lett. 93 (8) (2013) 473–480.
[32] Y. Komura, K. Tokunaga, Structural studies of stacking variants in Mg-base Friauf–Laves phases, Acta Crystallogr. Sect. B Struct. Crystallogr. Cryst. Chem. 36 (7) (1980) 1548–1554.
[33] Y.Z. Ji, A. Issa, T.W. Heo, J.E. Saal, C. Wolverton, L.Q. Chen, Predicting β′ precipitate morphology and evolution in Mg–RE alloys using a combination of first-principles calculations and phase-field modeling, Acta Mater. 76 (2014) 259–271.
[34] A. Ramazani, S. Kazemiabnavi, R. Larson, Quantification of ferrite-martensite interface in dual phase steels: a first-principles study, Acta Mater. 116 (2016) 231–237.
[35] J.P. Perdew, K. Burke, M. Ernzerhof, Generalized gradient approximation made simple, Phys. Rev. Lett. 77 (18) (1996) 3865–3868.
[36] G. Kresse, J. Furthmüller, Efficient iterative schemes for ab initio total-energy calculations using a plane-wave basis set, Phys. Rev. B 54 (16) (1996) 11169–11186.
[37] P.E. Blöchl, Projector augmented-wave method, Phys. Rev. B 50 (24) (1994) 17953.
[38] G. Kresse, D. Joubert, From ultrasoft pseudopotentials to the projector augmented-wave method, Phys. Rev. B 59 (3) (1999) 1758.
[39] A. Biswas, D.J. Siegel, C. Wolverton, D.N. Seidman, Precipitates in Al–Cu alloys revisited: atom-probe tomographic experiments and first-principles calculations of compositional evolution and interfacial segregation, Acta Mater. 59 (2011) 6187–6204.
[40] A. Biswas, D.J. Siegel, D.N. Seidman, Simultaneous segregation at coherent and semicoherent heterophase interfaces, Phys. Rev. Lett. 105 (2010) 076102.
[41] S. He, P. Peng, L. Peng, Y. Chen, H. Wei, Z.Q. Hu, An interplay of sulfur and phosphorus at the γ-Ni/γ′-Ni_3Al interface, J. Alloys Compd. 597 (2014) 243–248.
[42] H.L. Wang, J.J. Tang, Y.J. Zhao, J. Du, First-principles study of Mg/Al_2MgC_2 heterogeneous nucleation interfaces, Appl. Surf. Sci. 355 (2015) 1091–1097.
[43] K. Li, Z.G. Sun, F. Wang, N.G. Zhou, X.W. Hu, First-principles calculations on Mg/Al_4C_3 interfaces, Appl. Surf. Sci. 270 (2013) 584–589.